Chung Yuan Journal
Vol. 26. No. 1, 1998. pp. 7-15

Steady Buoyant Droplets with Circulation and Surface Tension

SHIN-SHIN KAO

Department of Mathematics, Chung Yuan Christian University, Chung-Li, Taiwan 32023.
Email: skao@math.cycu.edu.tw.

(Received: December 18, 1997; Accepted: February 27, 1998)

ABSTRACT

Numerical solutions are presented for the steady flow corresponding to a two-dimensional moving droplet with circulation subject to the gravity and surface tension force. Solutions to the nondimensionalized system depend on four parameters-- the Atwood number A, the Froude number $\sqrt{c}$, the surface tension coefficient τ, and the intensity of vorticity inside the droplet Ω. The roles of these parameters in determining the stationary solution are studied. It is found the droplet is less deformed with larger $|\Omega|$ and τ. Features of the surrounding flow in selected combinations of the parameters are discussed, and numerical computations are confirmed by pertubation analysis for small A.

Key words: *Atwood number, Froude number, surface tension, vorticity, steady state, circulation.*

I. INTRODUCTION

A 2D fluid droplet of density ρ_1 surrounded by an unbounded fluid of different density ρ_2 experiences a buoyancy force $\boldsymbol{F}_g=-g(\rho_1-\rho_2)a\hat{\boldsymbol{y}}$ in which a is the area of the droplet. One possibility for balancing this buoyancy force is through the lift of the Magnus effect. If the droplet is moving at speed U in the x-direction and has circulation Γ and if the ambient fluid is irrotational, then this lift force is $\boldsymbol{F}_l=-\Gamma U\rho_2\hat{\boldsymbol{y}}$. Thus there is a balance between these two forces if

$$\Gamma U=-ga(\rho_1-\rho_2)/\rho_2. \tag{1.1}$$

A new class of steady, 2D vortical flows for which there is a balance between the buoyancy force $\boldsymbol{F}_g$ and the lift force $\boldsymbol{F}_l$ has been numerically constructed and analytically confirmed by the author and R. Caflisch [2]. In [2], the fluids are incompressible and inviscid, and the outer fluid is assumed to be irrotational. Within this "flying droplet" the vorticity $-\Omega$ is assumed to be a uniform constant; while the droplet boundary may consist of a vortex sheet of net circulation Γ_s. The total circulation of the droplet is then $\Gamma=-a\Omega+\Gamma_s$. Only symmetric solutions were investigated in [2], probably due to the same restriction pointed out in [1].

The resulting solutions in [2] show several interesting features. First of all, these flows are of Prandtl-Batchelor type, which are flows of a single fluid consisting of regions of constant vorticity surrounded by vortex sheets. After nondimensionalization, the solution is found to depend on three parameters: the Atwood number $A=(\rho_1-\rho_2)/(\rho_1+\rho_2)$, the interior vorticity Ω, and the squared Froude number c. When $A=0$, the solution is just a circular droplet with purely rotating flow. For the simple case $\Omega=0$, the solution does not depend on the parameter c. Secondly, as the Atwood number A increases from zero, the droplet boundary remains smooth until a critical value of A, denoted by $A=A_{lim}$, is reached at which the boundary develops two corners. The sheet strength γ is not differentiable at these corners. Thirdly, larger values of $|\Omega|$ result in larger $A=A_{lim}$'s, and examination of the tangential velocity shows that the two corners on the profiles at $A=A_{lim}$ are stagnation points. More specifically, it is found that the geometric character of the flow is related to the Atwood number in the following way. For small A, there is a single stagnation point in the exterior flow. At a particular value of A, this stagnation point hits the droplet boundary. For larger A values it splits into two stagnation points on the boundary, which are at the droplet corners at $A=A_{lim}$ (Fig. 1 of [2]). The corner angle is shown to be $2\pi/3$ both numerically and analytically. Finally the dependence of the solution on the Froude number $\sqrt{c}$ is very mild.

In this paper, we shall take into account the influence of the surface tension force and consider that our research in [2] is the special case where the surface tension is zero. Since the dependence upon c is again very mild, we simply show the results for $c=1$ and concentrate on how

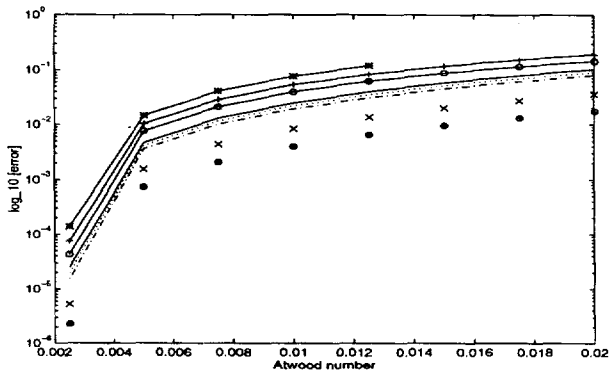

Fig. 1. The error curves for cases of different combinations of $|\Omega|$ and τ. Section III.A mentions how different symbols correspond to different cases.

the relation among the three parameters A, Ω and the surface tension coefficient τ affects the steady state solutions, inluding the shape of the droplet and the characters of the surrounding flow. Section 2 presents the formulation obtained by both the Eulerian and Lagrangian formulations, and performs perturbation analysis on the former and numerical iteration on the latter. Results obtained by section 2, and how the solutions imply about the nature of the flow are presented in section 3. There we show that solutions by the two different methods agree with each other, which verifies the validity of both approaches. Section 4 gives the conclusion of the whole study.

II. PROBLEM FORMULATION

We shall consider the steady state of a two-dimensional inviscid, incompressible droplet of one fluid surrounded by a second fluid under the influence of gravitational acceleration, and the surface tension. Since this work is closely related to the recent paper by the author ([2]), where the steady state of such droplets without surface tensions was studied, the readers might refer to [2] for a complete understanding of the derivation of formulation.

A. Eulerian Formulation

Assume that there is constant vorticity in the interior and that the droplet boundary is a vortex sheet. Let subscripts 1 and 2 represent fluid properties inside and outside the boundary, respectively, and the gravity acceleration g act in the negative y-direction. ρ_i, P_i, $\boldsymbol{u}_i$ denote the density, pressure, and velocity fields for i=1,2. The constant values of inner vorticity and vortex sheet circulation are denoted by $-\Omega$ and Γ_s, respectively.

The governing equations in Eulerian coordinates are the following:

$$\rho_i(\boldsymbol{u}_i\cdot\nabla)\boldsymbol{u}_i+\nabla P_i=-g\rho_i\hat{\boldsymbol{y}} \quad (x,y)\notin\partial D \tag{2.1}$$

$$\nabla\cdot\boldsymbol{u}_i=0$$

$$P_1+\tau k=P_2 \quad (x,y)\in\partial D \tag{2.2}$$

$$\boldsymbol{u}_i\cdot\boldsymbol{n}=0.$$

$$\boldsymbol{u}_2\to(U,0) \text{ dt } \infty$$

In (2.1) and (2.2), ∂D is the boundary of the droplet, $\hat{\boldsymbol{y}}$ is the unit vector in the positive y-direction, and $\boldsymbol{n}$ is the unit normal vector on ∂D. The readers might consider that the work in [2] is a special case with τ=0 in the Laplace's boundary condition in (2.2).

A particular simple solution of this system with $\rho_1=\rho_2$ is the following:

$$\partial D=\{(x,y):x^2+y^2=1\}$$

$$\begin{aligned}
\boldsymbol{u}_1 &= -\frac{r}{2}\Omega\hat{\boldsymbol{\theta}}\\
\boldsymbol{u}_2 &= \frac{\Gamma}{2\pi r}\hat{\boldsymbol{\theta}}\\
P_1 &= -g\rho_1 y+\frac{\Omega^2}{8}\rho_1 r^2-\frac{\Gamma}{8\pi^2}\rho_1\\
P_2 &= -g\rho_2 y-\frac{\Gamma}{8\pi^2}\rho_2\frac{1}{r^2}+\frac{\Omega^2}{8}\rho_2+\tau k
\end{aligned} \tag{2.3}$$

in which $\Gamma=-\Omega\pi+\Gamma_s$ is the total circulation, r, θ are variables in the polar coordinates and $\hat{\boldsymbol{r}}$, $\hat{\boldsymbol{\theta}}$ are unit vectors. This simple solution will be used as a basic solution from which to construct a perturbation expansion.

When the densities are different, the buoyancy force $\boldsymbol{F}_g=-g(\rho_1-\rho_2)\pi\hat{\boldsymbol{y}}$ acted on the droplet is balanced by the lift force $\boldsymbol{F}_l=-\Gamma U\rho_2\hat{\boldsymbol{y}}$ due to the Magnus effect, where U is the uniform velocity in the x-direction of the far-field flow, and the surface tension τk. Let the perturbed solution to (2.1), (2.2) for $\rho_1\neq\rho_2$ take the form ($\hat{\boldsymbol{x}}$, $\hat{\boldsymbol{z}}$ are unit vectors in the positive x and z directions):

$$\partial D=\{(r,\theta):r=R(\theta)\}$$

$$\begin{aligned}
\boldsymbol{u}_1 &= -\frac{r}{2}\Omega\hat{\boldsymbol{\theta}}+\nabla\times(\psi_1\hat{\boldsymbol{z}})=\nabla\times(\Psi_1\hat{\boldsymbol{z}})\\
\boldsymbol{u}_2 &= -\frac{\Gamma}{2\pi r}\hat{\boldsymbol{\theta}}+U\hat{\boldsymbol{x}}+\nabla\times(\psi_2\hat{\boldsymbol{z}})=\nabla\times(\Psi_2\hat{\boldsymbol{z}})\\
P_1 &= -g\rho_1 y+\tilde{P}_1\\
P_2 &= -g\rho_2 y+\tilde{P}_2
\end{aligned} \tag{2.4}$$

In (2.4), Ψ_i is the stream function in fluid i such that $\boldsymbol{u}_i=(\frac{\partial\Psi_i}{\partial y},-\frac{\partial\Psi_i}{\partial x})$, i=1,2. It is given by

$$\Psi_1 = \psi_1 + \frac{1}{4}r^2\Omega$$

$$\Psi_2 = \psi_2 + Uy - \frac{\Gamma}{2\pi}\log r. \tag{2.5}$$

Since ∂D is a streamline, we can set $\Psi_1=\Psi_2=0$ on ∂D. Also note that Γ, Ω are constants, and the area and center of the droplet is fixed as

$$\frac{1}{2}\int_0^{2\pi} R^2(\theta)d\theta = \pi. \tag{2.6}$$

$$\int_0^{2\pi} R(\theta)(\cos\theta, \sin\theta)d\theta = (0,0) \tag{2.7}$$

The system (2.1), (2.2) is solved by doing expansions around the special solution at $\rho_1=\rho_2$; i.e.

$$\rho_1=\rho_2+\epsilon$$

$$R=1+\epsilon R_1+\epsilon^2 R_2+...$$

$$\psi_i=\psi_{i0}+\epsilon\psi_{i1}+\epsilon^2\psi_{i2}+..., \quad i=1,2 \tag{2.8}$$

$$U=0+\epsilon U_1+\epsilon^2 U_2+...$$

$$B=B_0+\epsilon B_1+\epsilon^2 B_2+...$$

The unknown coefficient functions of ϵ^k in the above expansions are solved by further expanding them as Fourier sums of $\sin(k\theta)$ and $\cos(k\theta)$. The resulting solution, up to $O(\epsilon^2)$ terms, is

$$B \simeq \frac{1}{8}\rho^2(\Omega^2 - (\Gamma/\pi)^2) + \epsilon\Omega^2/8 - \epsilon^2\rho_2 d_1^2$$

$$R(\theta) \simeq 1 + \epsilon^2 e_2 r^2\cos 2\theta$$

$$\psi_1(r,\theta) \simeq -\Omega/4 - \epsilon^2\frac{1}{2}\Omega e_2 r^2\cos 2\theta$$

$$\psi_2(r,\theta) \simeq \epsilon d_1 r^{-1}\sin\theta + \epsilon^2\frac{\Gamma}{2\pi}e_2 r^{-2}\cos 2\theta$$

$$U \simeq -\epsilon d_1$$

$$e_2 = 4\rho_2(g\pi/\rho_2\Gamma)^2 / \{\rho_2(\Omega^2 + \frac{\Gamma^2}{\pi^2}) + 12\tau\}$$
$$d_1 = g\pi/(\Gamma\rho_2). \tag{2.9}$$

Thus the shape of the droplet $\partial D=\{(x,y)(\theta)|0\le\theta<2\pi\}$ is obtained as

$$x(\theta)=R(\theta)\cos\theta$$
$$\simeq \cos\theta + \frac{\epsilon^2}{2}e_2\cos\theta + \frac{\epsilon^2}{2}e_2\cos(3\theta) \tag{2.10}$$
$$y(\theta)=R(\theta)\cos\theta$$
$$\simeq \sin\theta + \frac{\epsilon^2}{2}e_2\sin\theta + \frac{\epsilon^2}{2}e_2\sin(3\theta). \tag{2.11}$$

B. Lagrangian Formulation

We shall work in the complex $z=x+iy$ plane. The boundary of the droplet ∂D is described by the complex single-valued function $Z(\alpha)=X(\alpha)+iY(\alpha)$, which encloses a connected region D of fluid of constant vorticity $-\Omega$. The parameterization is in the clockwise direction, $0\le\alpha<2\pi$. The velocity field on ∂D, $q(Z)=(u+iv)(Z)$, is as in [2]:

$$\bar{q}(\alpha) = \frac{1}{2\pi i}PV\int_0^{2\pi}\frac{\gamma' - \Omega i\bar{Z}'Z'_\alpha/2}{Z(\alpha)-Z'}d\alpha' + \frac{\Omega i}{4}\bar{Z}(\alpha) + U. \tag{2.12}$$

The quantities with primes in the integral term in (2.12) are functions of the integration variable α'. $\gamma(\alpha')$ is the sheet strength with $\int_0^{2\pi}\gamma(\alpha')d\alpha'=\Gamma_s$. $PV\int$ denotes the Cauchy principal-valued integration since the integration in (2.12) is singular when $\alpha'=\alpha$.

The equation for $\gamma(\alpha)$ is derived by using the Bernoulli equations:

$$\frac{1}{2}|u_1|^2 + \frac{P_1}{\rho_1} + gy - \Psi_1\Omega = B_1 \quad (x,y) \text{ inside } \partial D \tag{2.13}$$

$$\frac{1}{2}|u_1|^2 + \frac{P_2}{\rho_2} + gy = B_2 \quad (x,y) \text{ outside } \partial D \tag{2.14}$$

in which the constants B_i's have no relation with the expansion coefficients in (2.8). By taking equations (2.13) and (2.14) on ∂D and eliminating the pressure terms by the boundary condition $P_1+\tau k=P_2$ in (2.2), we obtain

$$\gamma\mathrm{Re}\left[\frac{q}{Z_\alpha}\right] + A\left(\frac{\gamma^2}{4|Z_\alpha|^2} + \bar{q}q + 2gy\right) + \frac{\tau k}{\rho^2}(A-1) = B. \tag{2.15}$$

Here $A=(\rho_1-\rho_2)/(\rho_1+\rho_2)$ is the Atwood number, and B is a constant involving Ω, Ψ, ρ_i and B_i, i=1,2. The boundary condition $\boldsymbol{u}_i\cdot\boldsymbol{n}=0$ yields

$$\mathrm{Im}\left[\frac{q}{Z_\alpha}\right] = 0. \tag{2.16}$$

Next we nondimensionalize the problem by setti

$$Z = L\tilde{Z},\ \gamma = \frac{L^2}{T}\tilde{\gamma},\ q = \frac{L}{T}\tilde{q},\ U = \frac{L}{T}\tilde{U},\ \Omega = \tilde{\Omega}/T,\ B = \frac{L^2}{T^2}\tilde{B},$$
$$\Gamma = \frac{L^2}{T}\tilde{\Gamma},\ A = \frac{L}{gT^2}\tilde{A},\ \tau = \frac{L^3\rho_2}{T^2}\tilde{\tau}, \text{ and } k = \frac{1}{L}\tilde{k}, \text{ where all}$$

variables with "~" are the dimensionless quantities. The length scale L is chosen so that the area of the droplet is fixed, as in the Eulerian formulation.

$$\int_0^{2\pi}\tilde{y}d\tilde{x} = \pi. \tag{2.17}$$

The time scale T is then chosen so that the total circulation is -1; i.e.

$$\tilde{\Gamma} = -1. \tag{2.18}$$

Defining $c = \frac{L}{gT^2}$, which equals the square of the Froude number, and dropping "~", the resulting non-dimensional system is

$$\bar{q}(\alpha) = \frac{1}{2\pi i} PV \int_0^{2\pi} \frac{\gamma' - \Omega i \bar{Z}' Z'_\alpha / 2}{Z(\alpha) - Z'} d\alpha' + \frac{\Omega i}{4} \bar{Z}(\alpha) + U \tag{2.19}$$

$$\gamma \mathrm{Re}\left[\frac{q}{Z_\alpha}\right] + A\left(c\left(\frac{\gamma^2}{4|Z_\alpha|^2} + \bar{q}q\right) + 2y\right) + \tau k(cA - 1) = B \tag{2.20}$$

$$\mathrm{Im}\left[\frac{q}{Z_\alpha}\right] = 0 \tag{2.21}$$

$$\int_0^{2\pi} y dx = \pi \tag{2.22}$$

$$\int_0^{2\pi} \gamma d\alpha' = -1 + \Omega\pi \tag{2.23}$$

$$\int_0^{2\pi} (\mathrm{Re}\,(Z(\alpha)),\ \mathrm{Im}\,(Z(\alpha)))d\alpha = (0,0) \tag{2.24}$$

C. Numerical Method

The nonlinear system (2.19)-(2.24) in Lagrangian variables is numerically solved by the collocation method as in [2], where only solutions symmetric about the imaginary axis x=0 are sought.

The basic unperturbed solution to equations (2.19)-(2.24) for A=0 is given by

$$Z(\alpha) = \sin\alpha + i\cos\alpha$$

$$\gamma(\alpha) = \frac{\Omega}{2} + \frac{\Gamma}{2\pi}$$

$$q(\alpha) = -\frac{\Omega i}{4} Z(\alpha) + \frac{\Gamma i}{4\pi \bar{Z}(\alpha)}$$

$$U = 0$$

$$B = \left(\frac{\Omega}{2} + \frac{\Gamma}{2\pi}\right)\left(\frac{\Omega}{4} - \frac{\Gamma}{4\pi}\right) + \tau \tag{2.25}$$

The total circulation is fixed by setting Γ=-1. The solution to (2.19)-(2.24) is expressed in Fourier expansion around the known solution in (2.25); i.e.

$$Z(\alpha) = \sin\alpha + i\cos\alpha + X_1 \sin\alpha + i\sum_{j=1}^{N-1} Y_j \cos(j\alpha) \tag{2.26}$$

$$\gamma(\alpha) = \frac{\Omega}{2} - \frac{1}{2\pi} + \sum_{j=1}^{N-1} C_j \cos(j\alpha).$$

Note that equation (2.19) serves as a definition of $\bar{q}$, and (2.23) and (2.24) are automatically satisfied by using (2.26). There are 2N+1 unknowns $\{Y_j, C_j, j=1,2,...,N-1; X_1, B, U\}$. Evaluating (2.20), (2.21) at N points $\alpha_{k-1/2} = (k - \frac{1}{2})\frac{\pi}{N}$ for k=1,2,...,N, plus (2.22), results in a total of 2N+1 equations. We use the Newton's iterative scheme to solve this closed 2N+1 linear system, and the iteration stops when the absolute value of the difference between two successive iterative solutions is less then 10^{-7}. For specified values of Ω and τ, this problem is solved for various A for a typical value of N=128. The consistency of the computation is checked by showing the numerical solutions converge as the mesh size shrinks. Since Newton's iterative scheme converges quadratically, it takes usually 3 to 4 iterations to reach the 10^{-7} error bound. The continuation method is used for the initial guess in the Newton iteration. Also note that the horizontal and vertical positions are fixed by the property that $\int x d\alpha = \int y d\alpha = 0$.

III. RESULTS

A. Agreement between the Eulerian and Lagrangian Formulations

To demonstrate the validity of both the analytic and numerical results, we perform a comparison of the (analytical) Eulerian and (numerical) Lagrangian solutions. Here we will cast the analytical solution (using θ as a variable) into Lagrangian form (using α as a variable). The transformation is derived in [2], so we simply quote the final results:

$$X_1 = -Y_1 = \epsilon^2 e_2$$

$$Y_2 = O(\epsilon^3). \tag{3.27}$$

To use (3.27), we must relate $\epsilon = \rho_1 - \rho_2$ and the Atwood number A. We nondimensionalize ϵ as $\tilde{\epsilon} = \epsilon / \rho_2 = \frac{\rho_1 - \rho_2}{\rho_2}$ $= \frac{2A}{1-A}$. Also note that the solution for the nondimensional Eulerian formulation is the same except that g is replaced by $\frac{gT^2}{L} = c^{-1}$. Thus by choosing c=1, the analytical solution in Section 2.1 is nondimensionalized by setting g=1.

Using these values, we compare the results of the analytical and numerical solutions. In Table 1, there is a comparison of the values X_1 and Y_1 for the analytical and numerical solutions for Ω=0 at distinct τ, while A varies in a range of values. The "error" here is defined by $max(|analytical\ X_1 - numerical\ X_1|, |analytical\ Y_1 - \text{numerical}\ Y_1|)$. The numerical results for $\Omega = \pm 0.5$ and ± 1.0 show better agreement with the analytical values for small A. Table 2 presents the analytical and numerical solutions for τ=0.001 at different Ω's. We also find that the computa-

Table 1.

		numerical		analytical	
	A	X_1	Y_1	X_1=$-Y_1$	error
	.0025	.008690	-.008615	.008753	1.3777_{-4}
Ω=0.0	.0050	.034281	-.033145	.035189	2.0438_{-3}
τ=0.001	.0075	.075581	-.070270	.079574	9.3039_{-3}
	.0100	.131147	-.115942	.142180	2.6238_{-2}
	.0125	.199062	-.166015	.223282	5.7268_{-2}
		numerical		analytical	
	A	X_1	Y_1	X_1=$-Y_1$	error
	.0025	.006111	-.006074	.006149	7.4378_{-5}
Ω=0.0	.0050	.024147	-.023578	.024719	1.1405_{-3}
τ=0.005	.0075	.053193	-.050506	.055897	5.3909_{-3}
	.0100	.091982	-.084234	.099875	1.5641_{-2}
	.0125	.139119	-.122128	.156846	3.4718_{-2}
		numerical		analytical	
	A	X_1	Y_1	X_1=$-Y_1$	error
	.0025	.004459	-.004439	.004482	4.2374_{-5}
Ω=0.0	.0050	.017665	-.017358	.018017	6.5914_{-4}
τ=0.01	.0075	.039034	-.037568	.040743	3.1758_{-3}
	.0100	.067695	-.063403	.072799	9.3963_{-3}
	.0125	.102656	-.093099	.114325	2.1227_{-2}

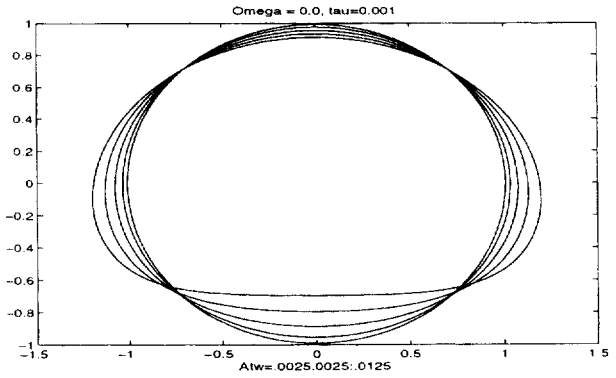

Fig. 2. The stationary profiles of the droplet at Ω=0.0, τ=0.001, at various A.

tional results for larger τ cases show better agreement with the analytical values for small A. The error curves for τ=0.001, 0.005, 0.010 for different Ω's are shown in Figure 1, where we plot the curves using different symbols for different cases --

Ω	τ	Symbol	Ω	τ	Symbol
0.0	0.001	-*-	0.5	0.001	-
	0.005	-+-		0.005	...
	0.010	-o-		0.010	-.
1.0	0.001	$\times$	1.5	0.001	$\oplus$

Table 2.

		numerical		analytical	
	A	X_1	Y_1	X_1=$-Y_1$	error
	.0025	.002713	-.002705	.002730	2.4674_{-5}
Ω=$\pm$0.5	.0050	.010777	-.010662	.010975	3.1354_{-4}
τ=0.001	.0075	.023973	-.023411	.024819	1.4080_{-3}
	.0100	.041004	-.040311	.044346	4.0357_{-3}
	.0125	.064594	-.060675	.069643	8.9675_{-3}
		numerical		analytical	
	A	X_1	Y_1	X_1=$-Y_1$	error
	.0025	.000886	-.000886	.000891	5.2555_{-6}
Ω=$\pm$1.0	.0050	.003535	-.003523	.003582	5.8243_{-5}
τ=0.001	.0075	.007921	-.007859	.008100	2.4045_{-4}
	.0100	.013999	-.013806	.014472	6.6592_{-4}
	.0125	.021716	-.021255	.022727	1.4723_{-3}
		numerical		analytical	
	A	X_1	Y_1	X_1=$-Y_1$	error
	.0025	.000417	-.000417	.000420	2.2788_{-6}
Ω=$\pm$1.5	.0050	.001668	-.001665	.001687	2.1880_{-5}
τ=0.001	.0075	.003745	-.003732	.003816	8.4038_{-5}
	.0100	.006639	-.006595	.006818	2.2226_{-4}
	.0125	.010335	-.010229	.010706	4.7716_{-4}

Table 3.

Ω=0 analyitical		numerical		
A	$-\epsilon d_1$	$U(\tau$=0.001)	$U(\tau$=0.005)	$U(\tau$=0.01)
.0025	.01574733	.01574733	.01574733	.01574733
.0050	.03157380	.03157380	.03157380	.03157380
.0100	.06346652	.06346652	.06346652	.06346652
.0200	.12822827	--	.12822827	.12822827
.0400	.26179939	--	.26179939	.26179939
.0800	.54636394	--	.54636394	.54636394

$\lvert\Omega\rvert$=0.5 analyitical		numerical		
A	$-\epsilon d_1$	$U(\tau$=0.001)	$U(\tau$=0.005)	$U(\tau$=0.01)
.0025	.01574733	.01574733	.01574733	.01574733
.0050	.03157380	.03157380	.03157380	.03157380
.0100	.06346652	.06346652	.06346652	.06346652
.0200	.12822827	.12822827	.12822827	.12822827
.0400	.26179939	.26179939	.26179939	.26179939
.0800	.54636394	.54636394	.54636394	.54636394

It is found that computational error decreases as $|\Omega|$ increases. Table 3 compares the numerically computed U with the exact analytical result U=$-\epsilon d_1$ and shows agreement to all significant digits. Similar results are observed for larger $|\Omega|$ computations.

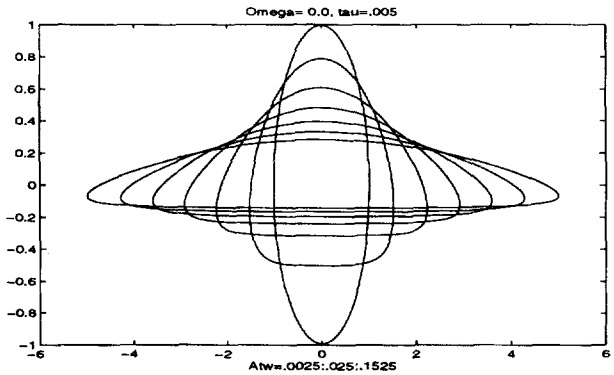

Fig. 3. The stationary profiles of the droplet at Ω=0.0, τ=0.005, at various A.

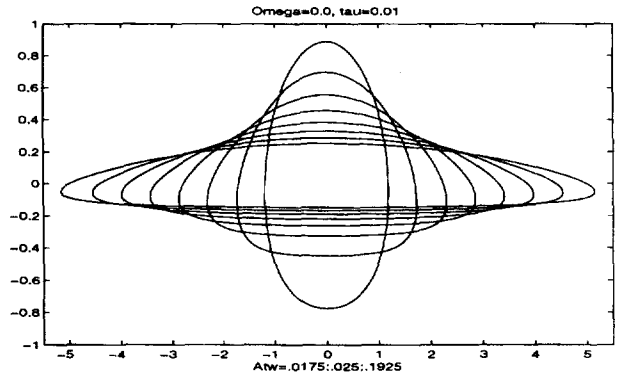

Fig. 4. The stationary profiles of the droplet at Ω=0.0, τ=0.01, at various A.

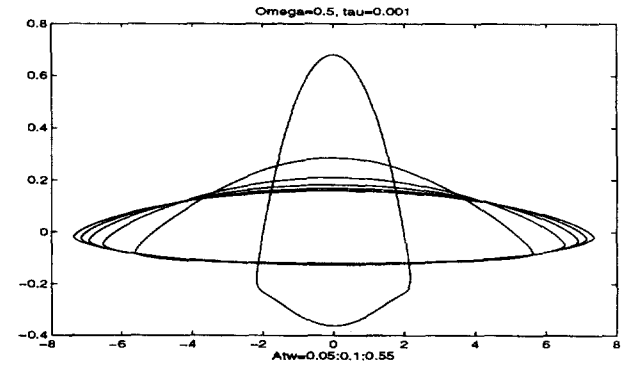

Fig. 5. The stationary profiles of the droplet at Ω=0.5, τ=0.001, at various A.

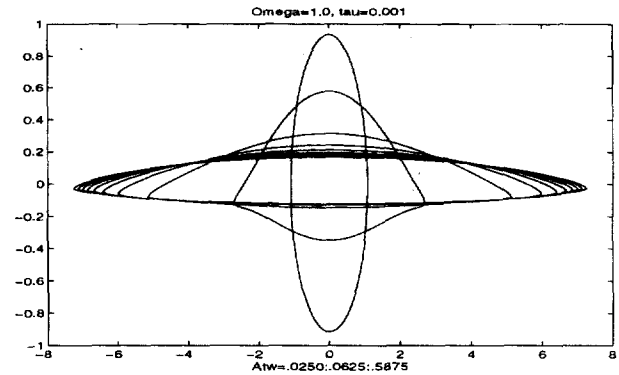

Fig. 6. The stationary profiles of the droplet at Ω=1.0, τ=0.001, at various A.

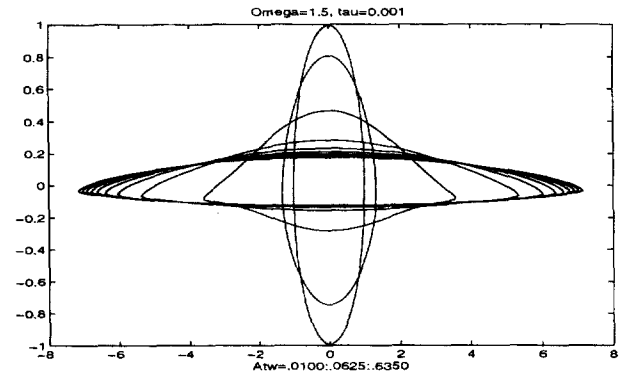

Fig. 7. The stationary profiles of the droplet at Ω=1.5, τ=0.001, at various A.

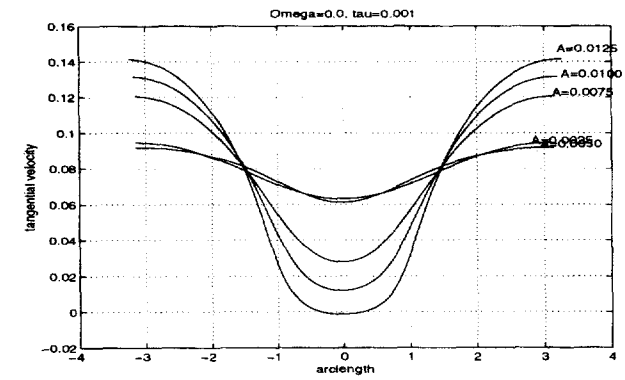

Fig. 8. The tangential velocity on the boundary vs. arclength for Ω=0.0, τ=0.001, at various A.

B. Discussion

Here we present the stationary profiles of the droplet and the corresponding velocity fields derived by our numerical results. In Figures 2 to 4, we plot the shape of the droplet at various A up to A_{lim}, beyond which the iteration fails to converge, for Ω=0 at τ=0.001, 0.005, and 0.01. In Figure 5 to 7, we show the stationary shape of the droplet for the case τ=0.001, Ω=$\pm$0.5, $\pm$1, and $\pm$1.5. Note that the scales on Figure 2 to 7 are not equal, thus indeed the stationary shapes at large A are very flat. Besides, both the analytical and numerical results show that the stationary

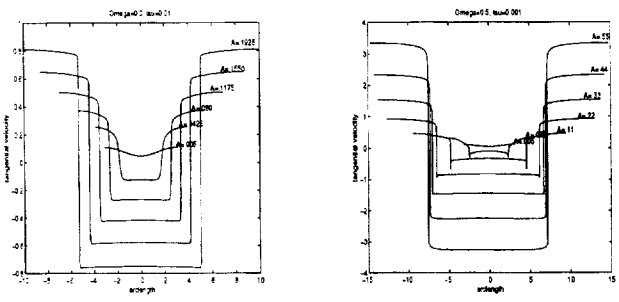

Fig. 9. The tangential velocity on the boundary vs. arclength for Ω=0.0, τ=0.01 (left), and Ω=0.5, τ=0.001 (right), at various A.

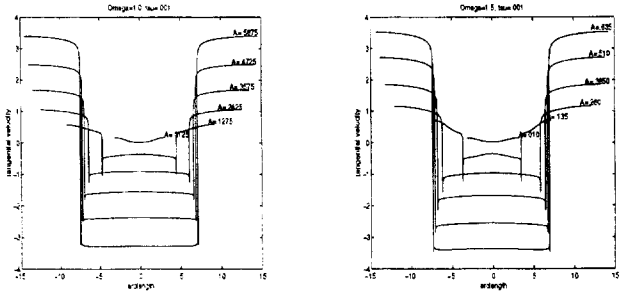

Fig. 10. The tangential velocity on the boundary vs. arclength for Ω=1.0, τ=0.001 (left), and Ω=1.5, τ=0.001 (right), at various A.

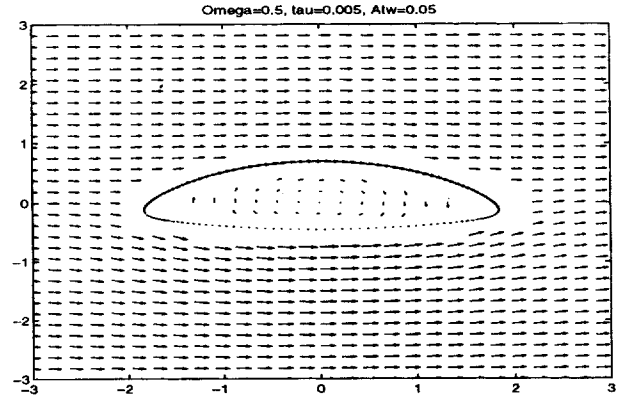

Fig. 11. The velocity field for Ω=0.5, τ=0.005, A=0.05.

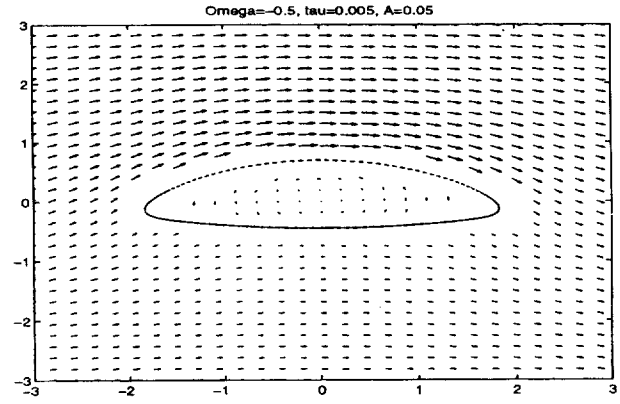

Fig. 12. The velocity field for Ω=-0.5, τ=0.005, A=0.05.

shapes are independent of the sign of Ω.

To realize the characters of the flow field in each case, we plot the corresponding tangential velocity field on the droplet boundary. Since the normal velocity on the boundary of a stationary droplet must be zero, a vanishing tangential velocity indicates the existence of a stagnation point on the boundary. Figure 8 to 10 show that for all combinations of Ω and τ in our tests, as A increases, the number of stagnation points changes from 0, to 1 and to 2. By checking of the arclength of the location of stagnation points and examining the velocity field of the surrounding flow, we find that as A is small, there is a stagnation point on the outside flow. As A increases, the stagnation point on the outside flow field moves to the middle point of the bottom of the droplet, then splits into to two, and the two move apart to the two corners on the boundary. Figure 11 and 12 show the velocity fields of two selected cases--Ω=$\pm$0.5, τ=0.005, and A=0.05. Both (2.8)-(2.11) and our computational results show that different signs of Ω correspond to identical shapes of the droplet and the same far-field velocity U, while the velocity fields inside the droplet are in opposite directions.

These results present similar observations of Pullin and Grimshaw [1] for nonlinear interfacial gravity waves in a two-layer Boussinesq fluid, in which the upper layer consists of a flow of constant vorticity and the lower layer is irrotational. They found that the appearance of the most extreme wave was consistent with that of one or more stagnation points on the wave profile. The observation that the droplet boundary is retained better for larger values of the interior vorticity was also found by Moore, Saffman, and Tanveer [3] in studying the Batchelor flows in the cases of the Sadovskii vortex and the rotational corner flow.

Finally, in contrast to the study in [2], where the stationary shapes at A_{lim} all contain singular points, our most limiting solutions obtained by numerical iteration still have smooth boundarys. Since it is well known that surface tension is a dispersive regularization of the Kelvin-Helmholtz and Rayleigh-Taylor instability near a stationary state (Drazin & Reid, 1981), and that numerical computation of interfacial flows with surface tension suffers from stiffness due to computing higher derivatives, our intuitive Newton's iterative method does require delicate modification to overcome such difficulties.

IV. CONCLUSIONS

We have set up the system describing a two-dimensional vortical droplet in an inviscid, incompressible fluid with circulation under the influence of gravity and surface tension force, using both Eularian and Lagrangian formulations. It is found that the non-dimensionalized system contains four parameters-A, $\sqrt{c}$, τ and Ω, yet the dependence on $\sqrt{c}$ is very mild.

A pertubation analysis was performed on the Eularian system to derive a class of stationary flows for small A, while numerical computations were done for several combinations of τ and Ω up to A_{lim}, beyond which the numerical method ceased to converge. Only symmetric solutions were sought. For small A, numerical solutions agree with analytical solutions well. It is found that the droplet is less deformed for larger $|\Omega|$'s and τ's and hence the corresponding A_{lim} increases. In all cases we tested for given Ω and τ, the most limiting solution contains two stagnation points on the boundary. The location of the stagnation points helped us to realize the surrounding flow field in each case. We also found that the far-field velocity U and the stationary shape of the droplet are independent of the signs of Ω, while the velocity field inside the droplet is opposite with different $sgn(\Omega)$.

There are two important issues related to this work. One is the stability analysis of the steady-state solutions found here. In Appendix, we prove that the solutions are linearly stable for small A for any given τ and Ω, using the exact solutions derived in Section 2.1. However, for larger A, being short of analytical form of the solutions prevent us from verifying their stability. One possible way of analyzing the stability for numerical results is to derive the Hamiltonian for this system and check whether our numerical answers give positive definite second variations. Another way is to use the corresponding time-dependent system and numerically investigate how these solutions will develop as time evolves if a small disturbance is introduced. This has been currently under study (S. Kao). The other issue is the stiffness due to the surface tension term. A refined numerical method must be suggested to handle such over-regularization, but a practical remedy is still an open problem.

APPENDIX: LINEAR STABILITY

The governing equations in Eulerian coordinates are the following:

$$\nabla^2\psi_1 = \Omega \tag{A.1}$$

$$\int \frac{\partial}{\partial y}(\frac{\partial}{\partial t}\psi_1)dx + \frac{1}{2}|\nabla\psi_1|^2 + \frac{P_1}{\rho_1} + gy - \psi_1\Omega = B_1 \tag{A.2}$$

$$\nabla^2\phi_2 = 0 \tag{A.3}$$

$$\frac{\partial}{\partial t}\phi_2 + \frac{1}{2}|\nabla\phi_2|^2 + \frac{P_2}{\rho_2} + gy = B_2 \tag{A.4}$$

Denote by ∂D the boundary of the droplet. Equations (A.1) and (A.2) are for (x,y) inside ∂D, while equations (A.3) and (A.4}) are for (x,y) outside ∂D. The first term in (A.2) can be replaced by $-\int \frac{\partial}{\partial x}(\frac{\partial}{\partial t}\psi_1)dy$. The boundary conditions are:

$$\vec{n}\cdot(\frac{\partial}{\partial t}\psi_1, -\frac{\partial}{\partial x}\psi_1) = \vec{n}\cdot\nabla^2\phi_2 \tag{A.5}$$

$$P_1 = P_2 \tag{A.6}$$

$$\nabla\phi_2 \to (U,0) \text{ at } \infty. \tag{A.7}$$

Here $\vec{n}$ is the normal vector on ∂D. [2] shows that steady state solutions exist when g and Γ are specified (we took g=1 and Γ=−1) and Ω is given for $0 \le A_{tw} < A_{lim}$, where A_{lim} is the extreme value beyond which the collocation method fails to converge. We shall denote by ψ_1^0, ϕ_2^0, P_1^0, P_2^0 and $R^0(\theta)$ the corresponding steady state stream function for inner flow, potential function for outer flow, the pressure distribution, and the boundary $\partial D=\{(r,\theta): r=R(\theta)\}$ for given fixed values of Ω, ρ_1 and ρ_2. Obviously, ψ_1^0, ϕ_2^0, P_1^0, P_2^0 and $R^0(\theta)$ satisfy equations (A.1)-(A.7). We perturb these functions by writing

$$\psi_1 = \psi_1^0 + \psi_1'$$

$$\phi_2 = \phi_2^0 + \phi_2'$$

$$P_i = P_i^0 + P_i', \quad i=1,2$$

$$R(\theta)=R_0(\theta)+R'(\theta). \tag{A.8}$$

Plugging (A.8) into equations (A.1)-(A.7), we obtain the equations for the perturbation functions:

$$\nabla^2\psi_1' = 0 \tag{A.9}$$

$$\int \frac{\partial}{\partial y}(\frac{\partial}{\partial t}\psi_1')dx + \nabla\psi_1^0\cdot\nabla\psi_1' + \frac{P_1'}{\rho_1} + gR'\sin\theta - \psi_1'\Omega = B_1' \tag{A.10}$$

$$\nabla^2\phi_2' = 0 \tag{A.11}$$

$$\frac{\partial}{\partial t}\phi_2' + \nabla\phi_2^0\cdot\nabla\phi_2' + \frac{P_2'}{\rho_2} + gR'\sin\theta = B_1'. \tag{A.12}$$

Again, equations (A.9), (A.10) are for (x,y) inside ∂D and (A.11), (A.12) for (x,y) outside ∂D. The boundary conditions are:

$$\vec{n}\cdot(\frac{\partial}{\partial y}\psi_1', -\frac{\partial}{\partial x}\psi_1') = \vec{n}\cdot\nabla\phi_2' \quad (A.13)$$

$$P_1' = P_2' \quad (A.14)$$

$$\nabla\phi_2' \to (0,0) \text{ at } \infty \quad (A.15)$$

Taking (A.10), (A.12) to ∂D and cancel the pressure term by (A.14), we derive:

$$\rho_2\frac{\partial}{\partial t}\phi_2' + \rho_2\nabla\phi_2^0\cdot\nabla\phi_2' + (\rho_2-\rho_1)gR'\sin\theta$$
$$-\rho_1\int\frac{\partial}{\partial y}(\frac{\partial}{\partial t}\psi_1')dx - \rho_1\nabla\psi_1^0\cdot\nabla\psi_1' + \rho_1\psi_1'\Omega = \tilde{B}, \quad (A.16)$$

where $\tilde{B} = \rho_2 B_2' - \rho_1 B_1'$.

Assume that $\psi_1' = \psi_1(r)e^{i(k\theta+ct)}$, and $\phi_1' = \hat{\phi}_2(r)e^{i(k\theta+ct)}$, where $i=\sqrt{-1}$, t is the time variable, k is an integer and c could be a complex number. (A.9), (A.11) and (A.15) imply that

$$\hat{\psi}_1(r) = Ar^{|k|} \quad (A.17)$$

$$\hat{\psi}_2(r) = Br^{|k|}, \quad (A.18)$$

where A and B are constants. We shall write k instead of $|k|$, assuming that k is nonnegative. We can use (A.13) to find the relation between A and B. Let $(X,Y)(\theta)$ denote a boundary point, i.e. $\partial D=\{(X,Y)(\theta): (X^2+Y^2)(\theta)= R(\theta)^2, 0\le\theta<2\pi$, then

$$\vec{n} = (\frac{\partial Y}{\partial\theta}, -\frac{\partial X}{\partial\theta})(\theta)$$
$$= (\frac{\partial R^0}{\partial\theta}\sin\theta + R^0\cos\theta, -\frac{\partial R^0}{\partial\theta}\cos\theta + R^0\sin\theta). \quad (A.19)$$

By (A.17)-(A.19), (A.13) implies that $A=iB$. Now we shall plug $\psi_1' = iBr^k e^{i(k\theta+ct)}$ and $\phi_2' = Br^{-k}e^{i(k\theta+ct)}$ into (A.16), which holds on $r=R^0(\theta)$.

In [2], we have shown that $R^0(\theta)=1+\epsilon^2 e_2\cos(2\theta)$, where $\epsilon=\rho_1-\rho_2$ and $e_2 = 4g^2\pi^2 / \{(\Omega^2 + \frac{\Gamma^2}{\pi^2})\Gamma^2\rho_2^2\}$ is a constant. Thus we can expand each term in (A.16) about $r=1$. For example,

$$\frac{\partial\phi_2'}{\partial t}\bigg|_{(r=R^0,\theta)} = \frac{\partial\phi_2'}{\partial t}\bigg|_{(r=1,\theta)} + \epsilon^2 e_2\cos(2\theta)$$
$$\cdot\frac{\partial}{\partial r}(\frac{\partial\phi_2'}{\partial t})\bigg|_{(r=1,\theta)} + \ldots$$

We collect the coefficients of each power of ϵ, and find that the $O(1)$ equation is the same as (A.16) except that the term containing the gravity is dropped, and it is now evaluated at $r=1$. The equation becomes:

$$\rho_2 Be^{iz}ic + \rho_2\frac{\Gamma}{2\pi}kBe^{iz}i + \rho_1 Bcie^{iz} - \rho_1\frac{\Omega}{2}kBie^{iz}$$
$$+\rho_1 Bie^{iz}\Omega = \tilde{B} \quad (A.20)$$

Here $z=k\theta+ct$. (A.20) implies that $\tilde{B}=0$ and $c=(\rho_1\Omega(k/2-1)-\rho_2\Gamma k/(2\pi))/(\rho_1+\rho_2)$ is a real number. Thus our perturbation functions all stay the same magnitude as time t proceeds. This proves the linear stability of the steady state solution at small Atwood number.

REFERENCES

1. R. H. J. Grimshaw and D. I. Pullin. Interfacial progresive gravity waves in a two-layer shear flow. J. Phys. Fluids 26(7), pp. 1731, 1983.
2. S. Kao and R. Caflisch. Steady buoyant droplet with criculation. J. Phys. Fluids.
3. D. W. Moore, P. G. Saffman, and S. Tanveer. The calculation of some Batchelor Flows:the Sadovskii vortex and rotational corner flow. J. Phys. Fluids 31(5), pp. 978, 1988.

含表面張力與環流的旋轉水珠之穩態解

高欣欣

中原大學數學系

臺灣省中壢市普仁 22 號

摘　要

針對二維理想流體中受環流、重力加速度及表面張力影響而移動的漩流水珠之穩定態，尋找數值模擬的答案。經過無量化(nondimensionalization)後的微分方程組僅含四個參數 --- 與密度比相關的 Atwood number (A)，與重力場有關的 Froude number ($\sqrt{c}$)，表面張力係數(τ)及水珠內部的漩渦強度(Ω)。本文研究此四參數在決定穩態解的型態所扮演的角色。結果顯示水珠的形狀在較大的 $|\Omega|$ 與 τ 時被較好地維持，而不易變形。參數數值不同的組合亦被選定來研究週圍流場的特性；在A值較小的範圍裡，數值結果皆以分析上的擾動理論加以印證。

本文的結果亦從定性上與其他相近研究比對，得到一致的結論。

關鍵詞：艾特伍數，弗若德數，表面張力，漩渦，穩態，環流。